Remote Sensing of Environment 148 (2014) 70–83

Contents lists available at ScienceDirect

Remote Sensing of Environment

journal homepage: www.elsevier.com/locate/rse

Urban tree species mapping using hyperspectral and lidar data fusion

Michael Alonzo *, Bodo Bookhagen, Dar A. Roberts

Geography Department, Ellison Hall 1832, UC Santa Barbara, CA 93106-4060, USA

ARTICLE INFO

Article history:
Received 28 October 2013
Received in revised form 19 March 2014
Accepted 23 March 2014
Available online xxxx

Keywords:
Data fusion
Tree species classification
Urban remote sensing
Lidar data
Hyperspectral imagery
Discriminant analysis
Watershed segmentation

ABSTRACT

In this study we fused high-spatial resolution (3.7 m) hyperspectral imagery with 22 pulse/m^2 lidar data at the individual crown object scale to map 29 common tree species in Santa Barbara, California, USA. We first adapted and parallelized a watershed segmentation algorithm to delineate individual crowns from a gridded canopy maxima model. From each segment, we extracted all spectra exceeding a Normalized Difference Vegetation Index (NDVI) threshold and a suite of crown structural metrics computed directly from the three-dimensional lidar point cloud. The variables were fused and crowns were classified using canonical discriminant analysis. The full complement of spectral bands along with 7 lidar-derived structural metrics were reduced to 28 canonical variates and classified. Species-level and leaf-type level maps were produced with respective overall accuracies of 83.4% (kappa = 82.6) and 93.5%. The addition of lidar data resulted in an increase in classification accuracy of 4.2 percentage points over spectral data alone. The value of the lidar structural metrics for urban species discrimination became particularly evident when mapping crowns that were either small or morphologically unique. For instance, the accuracy with which we mapped the tall palm species *Washingtonia robusta* increased from 29% using spectral bands to 71% with the fused dataset. Additionally, we evaluated the role that automated segmentation plays in classification error and the prospects for mapping urban forest species not included in a training sample. The ability to accurately map urban forest species is an important step towards spatially explicit urban forest ecosystem assessment.

1. Introduction

As of 2011, more than 50% of all humans live in cities (UN-Habitat, 2011). Cities play an outsized role in driving global climate change (Schneider, Friedl, & Potere, 2010) and are uniquely susceptible to climate change impacts. Urban areas suffer from higher temperatures, poorer air quality, and increased peak flow of stormwater runoff, when compared to their rural neighbors (Escobedo & Nowak, 2009; Lee & Bang, 2000; Voogt, 2002). Optimally arranged green infrastructure in cities can reduce impacts by facilitating reduced urban temperatures, improving air quality, and dampening peak flow (Bolund & Hunmammar, 1999; Myint, Brazel, Okin, & Buyantuyev, 2010). Urban trees in particular provide a range of ecosystem services, along with some disservices (e.g. Lyytimaki et al., 2008), but the magnitude of service depends on tree species, structure, and locational context (Escobedo & Nowak, 2009; Manning, 2008; McCarthy & Pataki, 2010, McPherson, Simpson, Xiao, & Wu, 2011; Simpson, 2002; Urban, 1992). Presently, the Urban Forest Effects model (UFORE, Nowak et al., 2008) is commonly implemented in urban areas worldwide to produce city-wide estimates of urban forest structure, species diversity, and ecosystem function. However, urban forest inventory, particularly on private properties, is labor intensive and the results are not spatially explicit.

Mapping the extents of urban tree canopy using aerial or satellite imagery is currently operational (MacFaden, O'Neil-Dunne, Royar, Lu, & Rundle, 2012; McGee, Day, Wynne, & White, 2012). However, these maps rarely provide information on tree species, age class, or leaf area index (LAI), which are common prerequisites to estimates of ecosystem function. Mapping tree species is challenging in urban environments due to the fine characteristic scale of spatial variation (Welch, 1982) and potentially very high species diversity. While some space-borne, broadband sensors (e.g., IKONOS, GeoEye) are capable of achieving <3 m multispectral spatial resolution, they lack the spectral range and resolution required to resolve the subtle chemical and structural signatures upon which species discrimination relies (Clark, Roberts, & Clark, 2005). Hyperspectral imagery has proven useful in mapping tree species at the pixel level based on variability in spectral reflectance at leaf to crown scales (Boschetti, Boschetti, Oliveri, Casati, & Canova, 2007; Clark et al., 2005; Dennison & Roberts, 2003; Franke, Roberts, Halligan, & Menz, 2009; Martin, Newman, Aber, & Congalton, 1998; van Aardt & Wynne, 2007; Yang, Everitt, Fletcher, Jensen, & Mausel, 2009; Youngentob et al., 2011). In an urban setting, Xiao, Ustin, and McPherson (2004) mapped 22 common species in Modesto, California with 70% accuracy at the species level and 94% accuracy at the leaf-type (i.e., broadleaf, conifer, palm) level.

* Corresponding author. Tel.: +1 805 883 8821.
E-mail address: mike.alonzo@geog.ucsb.edu (M. Alonzo).

http://dx.doi.org/10.1016/j.rse.2014.03.018
0034-4257/

Classification accuracies for pixel-based algorithms in highly mixed urban landscapes are limited by extreme spectral variation over small spatial extents. In response there has been increased use of object-based image analysis (OBIA), which relies on image segmentation routines to group spectrally similar and spatially proximate pixels into objects to reduce undesirable noise common in pixel-level results (Benz, Hofmann, Willhauck, Lingenfelder, & Heynen, 2004; Blaschke, 2010; Myint, Gober, Brazel, Grossman-Clarke, & Weng, 2011). This technique has been applied with some success to tree species identification using hyperspectral imagery either through crown-level spectral averaging or pixel-majority classification (Alonzo, Roth, & Roberts, 2013; Clark et al., 2005; van Aardt & Wynne, 2007; Zhang & Qiu, 2012). In a suburban setting north of Dallas, Texas, Zhang and Qiu (2012) achieved a classification accuracy of 69% for 40 tree species using a "treetop-based" approach. They selected the single highest pixel per crown object in order to ensure sunlit spectra whenever possible. Alonzo et al. (2013) showed that for manually delineated urban tree crowns in Santa Barbara, the pixel majority approach using all crown pixels exceeding a Normalized Difference Vegetation Index (NDVI) threshold was effective, especially with limited training data. Their classification of 15 urban species with Airborne Visible/Infrared Imaging Spectrometer (AVIRIS) data resulted in an overall accuracy of 86%. Nevertheless, Castro-Esau, Sanchez-Azofeifa, Rivard, Wright, and Quesada (2006), while producing strong species classification results using leaf-level spectra, show a linear decline in classification accuracies with increasing numbers of species. This suggests that 1) it may not be currently possible to map all species simultaneously in biodiverse forests and 2) that expanding the classification feature space with non-spectral data may be required for significant advances.

Lidar data allow for the generation of a set of crown structural variables based on either the ranges and intensities of individual pulse returns or characterization of the full waveform. Lidar data have been employed frequently to measure forest parameters such as tree height (e.g., Andersen et al., 2006; Edson & Wing, 2011; Lim, Treitz, Wulder, St-Onge, & Flood, 2003), biomass (e.g., Asner et al., 2011; Mascaro, Detto, Asner, & Muller-Landau, 2011; Næsset & Gobakken, 2008; Popescu, Wynne, & Nelson, 2003; Shrestha & Wynne, 2012), and LAI (e.g., Morsdorf, Kotz, Meier, Itten, & Allgower, 2006; Solberg et al., 2009; Tang et al., 2012; Zhao & Popescu, 2009). Classification of trees using pulse range and intensity metrics has been undertaken at the leaf type (e.g., Kim, Mcgaughey, Andersen, & Schreuder, 2009; Ørka et al., 2009; Yao, Krzystek, & Heurich, 2012), genus (e.g., Kim, Hinckley, & Briggs, 2011), and species levels (e.g., Brandtberg, 2007; Holmgren & Persson, 2004). Other work has shown that retaining the full lidar waveform can provide a set of discriminatory variables derived from, for example, echo width and amplitude (Heinzel & Koch, 2011; Vaughn, Moskal, & Turnblom, 2012). Suites of canopy structural variables (e.g. tree height, crown base height, vertical intensity profiles) extracted from the lidar point cloud at the individual tree level offer complementary information to the biochemical and biophysical data garnered from optical data. However, it has thus far not been demonstrated that lidar-variables alone are sufficient for discriminating among large numbers of species in biodiverse environments.

"Fusion" is a ubiquitous term in the remote sensing literature that generally refers to the combination of multisensor spatial data, at either the pixel, feature, or decision level (Pohl and Van Genderen, 1998). Increasingly, lidar and either multispectral (e.g., Holmgren, Persson, & Söderman, 2008; Ørka et al., 2012) or hyperspectral (e.g., Asner et al., 2008; Dalponte, Bruzzone, & Gianelle, 2008; Dalponte, Bruzzone, & Gianelle, 2012; Dalponte, Ørka, Ene, Gobakken, & Næsset, 2014; Jones, Coops, & Sharma, 2010; Liu et al., 2011; Voss & Sugumaran, 2008) data are fused together at the pixel or feature level for tree species classification and quantification of forest inventory parameters (e.g., Anderson et al., 2008; Clark, Roberts, Ewel, & Clark, 2011; Latifi, Fassnacht, & Koch, 2012; Lucas, Lee, & Bunting, 2008; Swatantran, Dubayah, Roberts, Hofton, & Blair, 2011). In some cases the value of fusion has come from the addition of structural variables (e.g., height, standard deviation of all height points within a pixel) that are minimally correlated with spectral bands (Dalponte et al., 2008; Dalponte et al., 2012; Jones et al., 2010; Voss & Sugumaran, 2008). In others, fusion has added value indirectly through improved image segmentation and crown-object creation (Alonzo et al., 2013; Dalponte et al., 2014; Voss & Sugumaran, 2008; Zhang & Qiu, 2012). However, to the authors' knowledge, there has been minimal research focused on improving tree species classification using crown-object level fusion of hyperspectral imagery and structural metrics extracted directly from the 3-D lidar point cloud. Moreover, the prospects for mapping an *entire*, biodiverse urban forest to the leaf-type level with hyperspectral-lidar data fusion, have not been evaluated. Finally, there is limited knowledge of how automated image segmentation impacts the accuracy of classification results in a highly complex urban environment.

The goal of this study is to improve the accuracy of tree species mapping in the biodiverse city of Santa Barbara, California, through crown-object level fusion of AVIRIS (Green et al., 1998) imagery and high point-density lidar data. This paper builds significantly on the work by Alonzo et al. (2013) which focused on classifying manually-delineated tree crowns using hyperspectral imagery. In particular, we now include lidar-derived structural metrics in classification algorithms and delineate crowns using watershed segmentation. The specific aims of this paper are:

1) For our urban study area, within crown objects delineated using watershed segmentation, classify 29 common tree species using crown-level fusion of hyperspectral imagery and lidar data.
2) Test the extent to which *all* of the urban forest's canopy can be classified to the leaf type level using classification functions developed for the 29 common species. Leaf-type level classification is frequently sufficient for parameterizing estimates of urban ecosystem function that are largely mediated by crown structure measurements and total leaf area.
3) Evaluate the impact of segmentation error on classification accuracy through comparison of results from automatically delineated and manually delineated crowns.
4) Isolate particular spectral regions and lidar-derived structural variables that hold promise for improving discrimination among urban tree species and leaf types.

Our study helps cities move closer to a spatially explicit accounting of the common species in their urban forest. Further, it facilitates better understanding of the spectral and structural contributions to species discrimination as well as the benefits and errors associated with object-oriented approaches.

2. Data and methods

2.1. Study area and sample

This study was conducted in downtown Santa Barbara, California (34.42° N, 119.69° W) (Fig. 1). Santa Barbara is a city of about 90,000 residents located on a coastal plain between the Pacific Ocean to the south and the Santa Ynez mountains to the north. It has a Mediterranean climate and supports a diverse mix of native, introduced, and invasive urban forest species. A spatial database maintained by the City of Santa Barbara contains one or more specimens from >450 species. In a Fall 2012 inventory following UFORE protocols, 105 plots were sampled and 108 species recorded. Despite this diversity, far fewer species provide the bulk of the city's canopy cover: In Santa Barbara, based on UFORE and municipal data, we estimate that approximately 70% of the study area's trees represent over 80% of the city's canopy area yet comprise fewer than 30 species.

This study's first objective was to map approximately 80% of Santa Barbara's canopy to the species level by training a classifier on 29 common species. The 80% canopy cover threshold was chosen based on

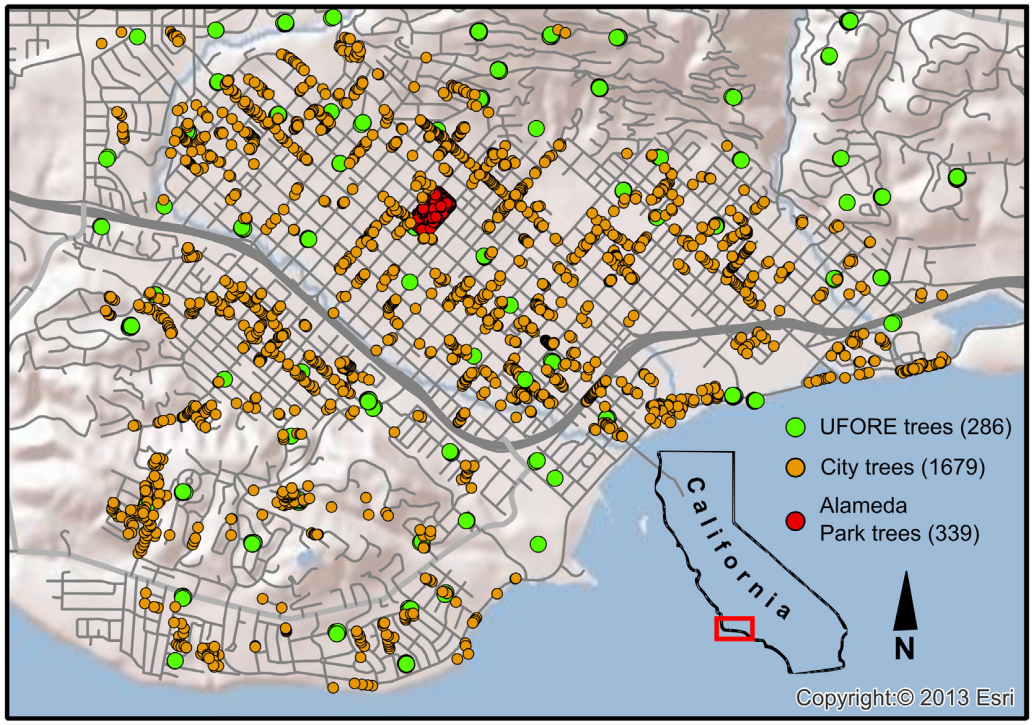

Fig. 1. Study area of downtown Santa Barbara (approximately indicated by red box overlaid on California locator map). Location of sampled trees shown by dots. (For interpretation of the references to color in this figure legend, the reader is referred to the web version of this article.)

analysis of UFORE-derived cumulative canopy cover distributions in the cities of Santa Barbara, Washington, DC (Casey Trees, 2010) and Los Angeles, California (Supplementary material Figure S1; Clarke, Jenerette, & Davila, 2013). Twenty nine species (Table 1) were ultimately chosen for their large contributions to canopy cover and our ability to isolate training crowns (Supplementary material S1). The other 20% of the canopy (hereafter "less common" species) were modeled as one of the trained species (hereafter "common" species) and thus classified only to the leaf-type level. The tree crowns included in this study's training set (Fig. 1) were selected from: 1) The city's geospatial database

Table 1
The 29 species included in model training. Tree type: B = Broadleaf, C = Coniferous, P = Palm. Canopy area refers to total canopy area by species.

Species code	Scientific name	Tree type	Stem count	Canopy area (m^2)
ARCU	*Archontophoenix cunninghamiana*	P	62	756
CICA	*Cinnamomum camphora*	B	57	5290
CUMA	*Cupressus macrocarpa*	C	55	4857
EUFI	*Eucalyptus ficifolia*	B	50	4596
EUGL	*Eucalyptus globulus*	B	58	9401
FIMI	*Ficus microcarpa*	B	56	9006
GEPA	*Geijera parviflora*	B	58	2777
JAMI	*Jacaranda mimosifolia*	B	76	6609
LIST	*Liquidambar styraciflua*	B	65	5081
LOCO	*Lophestemon confertus*	B	66	3465
MAGR	*Magnolia grandiflora*	B	63	7425
MEEX	*Metrosideros excelsa*	B	62	1581
OLEU	*Olea europaea*	B	81	6042
PHCA	*Phoenix canariensis*	P	99	5294
PICA	*Pinus canariensis*	C	73	4675
PIPI2	*Pinus pinea*	C	76	11,387
PIUN	*Pittosporum undulatum*	B	96	6166
PLRA	*Platanus racemosa*	B	71	6933
POGR	*Podocarpus gracilior*	B	62	6214
PYKA	*Pyrus kawakamii*	B	55	3404
QUAG	*Quercus agrifolia*	B	108	8895
SCMO	*Schinus molle*	B	53	1971
SCTE	*Schinus terebinthifolius*	B	71	5863
STSI	*Stenocarpus sinuatus*	B	51	1112
SYAU	*Syzygium australe*	B	67	3982
SYRO	*Syagarus romanzoffiana*	P	130	2705
TISP	*Tipuana tipu*	B	58	7874
ULPA	*Ulmus parvifolia*	B	50	6370
WARO	*Washingtonia robusta*	P	87	1220

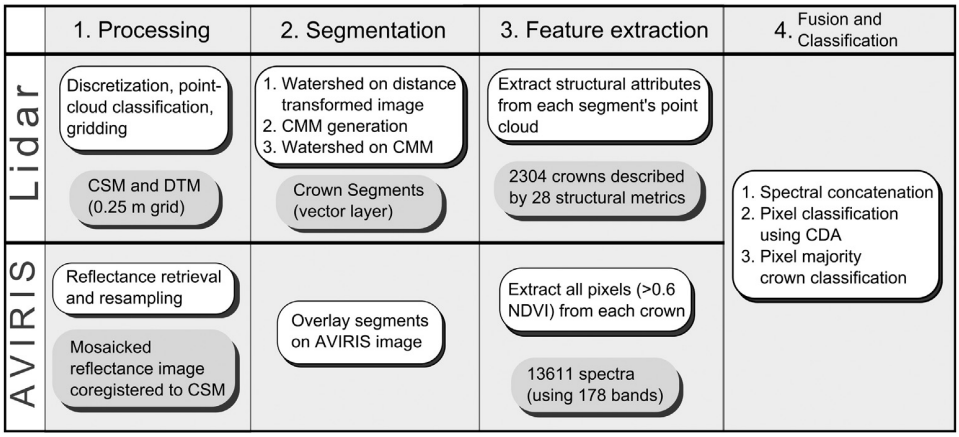

Fig. 2. Workflow diagram for data preprocessing, crown delineation via watershed segmentation, data fusion, and classification. White boxes are processes and gray boxes are data products. AVIRIS = airborne visible infrared imaging spectrometer, CSM = canopy surface model, DTM = digital terrain model, CMM = canopy maxima model, NDVI = normalized difference vegetation index, CDA = canonical discriminant analysis.

(1679 stems); 2) UFORE plots (286 stems);and 3) one additional park (Alameda Park) spanning two city blocks (339 stems). The species of each crown selected from the city's database was confirmed using Google Street View. The 2nd set was collected by the authors and included species identification and all UFORE-prescribed stem, crown, and positional measurements (Field methods in detail: https://sites.google.com/site/ucsbviperlab/uforemethods). The third set was also collected by the authors and each tree was identified to the leaf-type level with stem position precisely recorded using differential GPS and a total station. The primary utility of this final set was to offer a complex set of overlapping crowns on which to validate watershed segmentation algorithms. The total number of stems included in this analysis is 2304, comprising approximately 100 species. This number is approximate because not all species in Alameda Park were identified beyond their leaf type. Common species make up 2016 of the 2304 total crowns in the sample and 91% of the total crown area (165,887 m^2).

2.2. Data

2.2.1. Lidar data and processing

Waveform lidar data were collected in August of 2010 with a helicopter-mounted Riegl Q560 laser scanner. The lidar data were georeferenced with two local differential GPS stations and stored in the UTM coordinate system (Zone 11 N, NAD83). The waveform was discretized using standard Riegl processing procedures to an average last-return point density of 22 points/m^2 across the study area with additional returns available in high vegetation. Height values on flat surfaces were evaluated to be precise to within 2 cm (Supplementary material S2). The point cloud was classified to ground, building, and vegetation using LAStools (LAStools v111216, http://lastools.org) with minimal adjustments to default settings. Buildings were discriminated from trees with 98% accuracy and there was no confusion between vegetation taller than 2 m and ground. A bare earth digital terrain model (DTM), and two canopy height models (CHM), one for buildings and the other for vegetation, were generated at 0.25 m pixel resolution. In this research we use the term "canopy height model" to refer to height above bare ground.

2.2.2. AVIRIS imagery and processing

Two AVIRIS flight lines spanning the study area were acquired from a Twin Otter aircraft flying at approximately 4000 m above sea level on November 1, 2010. The scene acquisition times were centered on 11:50 and 14:20 Pacific Standard Time with solar zenith angles of 50.5° and 54.1°, respectively. The 224-channel AVIRIS instrument samples upwelling radiance between 365 and 2500 nm with a field of view of 34° and instantaneous field of view of 1 mrad (Green et al., 1998). The resultant ground instantaneous field of view was 3.7 and 3.4 m for the two flight lines, respectively.

AVIRIS products are delivered after correction for aircraft motion and orthorectification using digital terrain. Surface reflectance was retrieved on each flight-line using ATCOR-4 (Richter & Schlaepfer, 2002). Bands within the following spectral regions were discarded due to water vapor contamination or low signal-to-noise ratios: 365–385 nm, 1323–1432 nm, 1811–2007 nm, and 2446–2496 nm. After confirming negligible reflectance bias between the two images, a mosaic was created (3.7 m) and registered to the gridded lidar data (0.25 m). The AVIRIS data were warped using Delaunay triangulation based on 137 ground control points and resampled using nearest neighbor resampling. The average root mean square error (RMSE) in the alignment cannot be calculated automatically when Delaunay triangulation is employed. Visual assessment suggests that the error was less than one AVIRIS pixel.

2.3. Crown segmentation

A general overview of the segmentation process along with the full methods workflow employed for this study is shown in Fig. 2. In short, tree canopy was isolated from abiotic scene components and low vegetation primarily based on the point cloud classification completed in LAStools. Additional refinement was conducted using morphological opening, closing, thickening, and majority filtering on the gridded DTM and CHMs. This allowed for removal of most power lines, isolated vegetation canopies <1 m^2, and other image noise and resulted in a 0.25 m binary canopy image.

Building on the methods of Chen, Baldocchi, Gong, and Kelly (2006), marker-controlled watershed segmentation (Digabel & Lantuéjoul, 1978) was chosen to isolate individual tree crowns on the CHM. Additional background information on the watershed algorithm may be found in the Supplementary material (S3). For this project, we combined two watershed segmentation routines. The first was executed on an inverse distance transformed, binary canopy image, where local minima were marked at crown locations furthest from canopy edges. The second was executed on an inverted canopy maxima model (CMM) where markers were imposed in locations corresponding with maximum tree height. The second routine was enacted on each segment produced by the first routine thus further subdividing the initial segments. To create a CMM we used UFORE data to establish a local, empirical relationship between tree height and canopy width (Supplementary material S4). This linear model was used to establish a variable search window size for local crown maxima based on the modeled

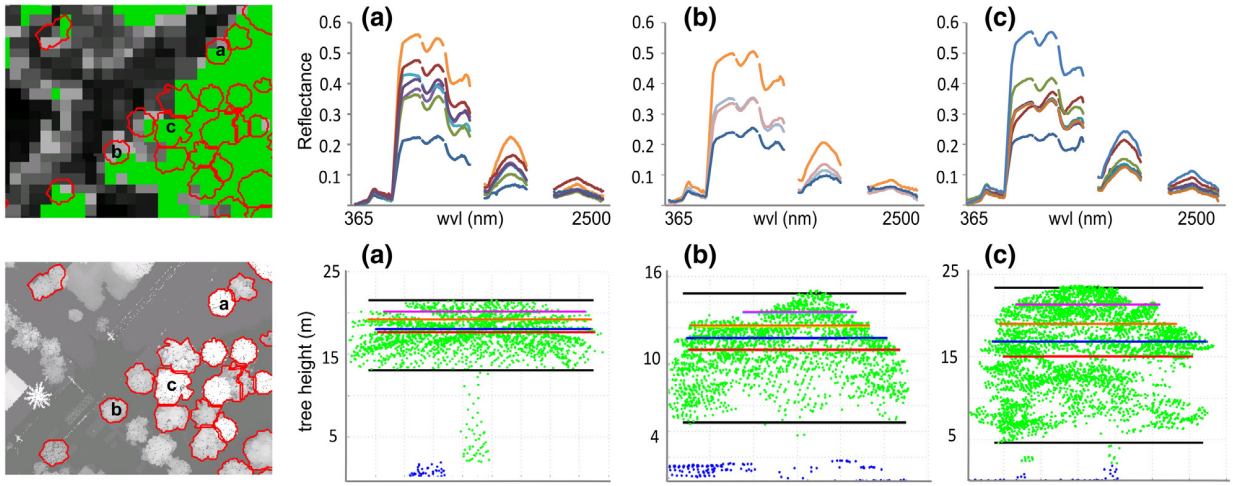

Fig. 3. *Top row*: Multiple AVIRIS spectra extracted from each of three typical watershed crowns. The green mask highlights pixels with NDVI > 0.6. The three example crowns are: a) PHCA (*Phoenix canariensis*), a palm; b) LOCO (*Lophostemon confertus*) a broadleaf evergreen; and c) PICA (*Pinus canariensis*), a conifer. *Bottom row*: Watershed crown point-cloud extraction with selected structural metrics. Black lines indicate crown base and max heights. Red line is mean crown height. Dark blue is median height of returns in crown. Orange and violet show 75th and 90th percentile heights as well as widths at those heights.

tree width. As an input to watershed segmentation, this method is considered an improvement over use of a CHM because it is more likely that only legitimate tree tops will be marked (Chen et al., 2006). However, the relationship between tree height and width in Santa Barbara's urban forest, irrespective of species was relatively weak ($r^2 = 0.38$).

Segmentation accuracy was estimated by calculating the ratio of field-measured stems contained in exactly one segment to the sum of the total number of stems and the number of segments containing zero stems. It was beyond the scope of this study to evaluate the areal accuracy of the segmentation. For further processing details and associated Matlab code relating to the watershed segmentation and CMM generation we refer the reader to Supplementary material S4.

2.4. Spectral and structural feature extraction

The following sections describe how the spectral and structural variables were generated from crown-level segments overlaid on the AVIRIS imagery and the lidar point cloud (Fig. 3). These variables were then fused and used to generate the classification models. Multiple AVIRIS spectra were extracted for each crown and a single set of 28 structural metrics were computed from each watershed-crown clipped point cloud. Section 2.5 on data fusion will discuss how these variables were combined for input into classification algorithms.

2.4.1. Extraction of spectra from AVIRIS imagery

Prior to extraction of spectra, the AVIRIS image was resampled from 3.7 m to 1 m resolution using nearest neighbor resampling. While this created redundant spectra, it was necessary to ensure that spectral information from valid 3.7 m canopy pixels located on segment edges was included in the analysis. Spectra were extracted from each crown segment (Fig. 3) using a variable NDVI (Rouse, Haas, Schell, & Deering, 1973) threshold to reduce contamination by impervious surface, soil, or non-photosynthetic vegetation spectral information. The average NDVI for all crowns was 0.61. Therefore, the initial extraction threshold was set to 0.6. If no pixels in a given crown met that criterion, all pixels above an NDVI of 0.5 were extracted. If no pixels met this second threshold, the single pixel with the maximum NDVI value was selected (Alonzo et al., 2013). All redundant spectra in a given crown segment were eliminated prior to classification. For our sample of 2304 crowns, 13,611 spectra were extracted with a median of 4 unique spectra per crown. Many of the species included in this study have small crowns that fully contain only one or two 3.7 m pixels. As such, 23% of crowns were represented in the classification stage by only one unique spectrum.

2.4.2. Extraction of structural metrics from lidar data

The lidar point-cloud subset associated with each tree crown was extracted from the scene tiles so that each crown could be processed individually (Fig. 3). This strategy allows for arbitrarily large tree crown datasets to be processed either in serial or with simple parallelization. Building upon previous work (e.g., Holmgren & Persson, 2004; Kim et al., 2009), we created 28 structural variables (Table 2). These metrics can be roughly categorized as relating to crown height (*h*), crown widths at selected heights (*w*), ratios of crown heights to widths at selected heights (*hw_rat*), direct measures of return intensity through the crown (*int*), distributions of intensity through the crown (*int_dist*) and crown porosity measured by return penetration into the crown (*cp*). Details and Matlab code relating to the computation of these variables can be found with the Supplementary material (S5). While overall correlation among variables was limited, there were several groupings exhibiting Pearson's Product Moment Coefficients (r) greater than 0.80 (Supplementary material S5, Table S1). In order to exclude correlated variables and to choose the most effective variables for species separability, forward feature selection (FFS) was employed.

2.4.3. Forward feature selection (FFS)

FFS is a method used to reduce a high-dimensional dataset that may contain redundant discriminating variables (Hoffbeck & Landgrebe, 1996). The one variable that best discriminates among classes is first added to the classification model based on its ability to minimize the model's misclassification rate (MCR). Each remaining variable is sequentially tested to assess which will, when combined with those already included, offer the greatest marginal decrease in MCR. Alonzo et al. (2013) previously showed that a reduced set of spectral variables did not yield classification accuracies higher than the full complement of 178 bands and performed no better computationally than a reduced set of canonical variates. Thus, for purposes of improving model classification accuracy, only lidar variables were winnowed for further use using FFS. However, it is also an objective of this research (aim #4) to explore the contributions of different spectral regions to species separability in an urban forest. As such, each spectral band's unique contribution to separability was evaluated based in-part on frequency of that band's selection. A more general measure of separability, assessed as the ratio of among class sums of squares to within class sums of squares (F-ratio; Clark et al., 2005), was also employed to isolate useful spectral

Table 2
Lidar-derived structural variables. Bold entries were selected for inclusion in classification models for watershed crowns.

Variable	Description
h_1	Max crown height
h_2	**Median height of returns in crown**
h_3	Crown surface height: 0.25 m spatial resolution
h_4	Crown surface height: 1 m spatial resolution
h_5	Crown base height
w_1	**Crown width at median height of returns in crown**
w_2	Crown width at 50th percentile height
w_3	Crown width at 75th percentile height
w_4	Crown width at 90th percentile height
hw_rat_1	Ratio of crown length to tree height
hw_rat_2	**Ratio of crown height to width: median height**
hw_rat_3	Ratio of crown height to width: 90th percentile height
hw_rat_4	Ratio of crown height to width: 75th percentile height
hw_rat_5	Ratio of width at 90th percentile height to mean height
hw_rat_6	Ratio of N-S width to E-W width
int_1	Average intensity above median height
int_2	**Average intensity below median height**
int_3	**Crown surface intensity: 0.25 m spatial resolution**
int_4	Crown surface intensity: 1 m spatial resolution
int_dist_1	Crown surface intensity/overall average crown intensity
int_dist_2	Skewness of intensity distribution through crown
int_dist_3	Surface intensity (0.25 m)/surface intensity (1 m)
int_dist_4	Return intensity above median crown height/below
cp_1	**Surface heights (0.25 m)/surface heights (1 m)**
cp_2	(Mean crown height - median height of returns)/crown height
cp_3	**Count of returns in 0.5 m vertical slice at 90th percentile height divided by width at that height**
cp_4	Count of returns in 0.5 m vertical slice at mean crown height divided by width at that height
cp_5	Count of returns in 0.5 m vertical slice at median height of crown returns divided by width at that height

regions and categories of structural metrics (e.g. all variables related to height).

To explore the sensitivity of the structural variables to crown segmentation error, FFS was run on both manually delineated crowns (hereafter manual crowns) and watershed segments (hereafter watershed crowns). FFS was run on each set 100 times with crowns randomly partitioned each run into training and validation sets to mitigate the impact of crown variability in the sample. The seven structural metrics that were chosen using manual crowns in more than 30% of the runs and that demonstrated minimal intercorrelation were retained for further use. Accordingly, the 7 most-frequently selected metrics exhibiting low correlation were chosen for the watershed crowns (Table 2).

2.5. Data fusion and classification

2.5.1. Fusing spectral and structural data at the crown level

In this study, the majority of tree crowns contained multiple, unique spectra meeting the 0.6 NDVI threshold. However, there was only *one* set of structural metrics extracted per crown (Fig. 3). Alonzo et al. (2013) demonstrated that retaining multiple pixels per crown and assigning a class to the crown object using a pixel majority ("winner-take-all") approach was more accurate than classification using a single, crown-mean spectrum. As such, for each crown, we chose to replicate the set of structural metrics to correspond with the number of extracted spectra. The resulting data matrix for manual crowns contained 12,773 rows and 206 columns, where each row represents a unique spectrum and each column contains either one of 178 spectral bands or one of 28 structural metrics. The same structure was created for the watershed crowns but with 13,317 rows.

2.5.2. Canonical discriminant analysis (CDA)

All classifications in this study were conducted using canonical variates in a linear discriminant analysis (LDA) classifier. LDA has proven useful previously in remote sensing research for separating highly overlapping classes in (e.g., Clark et al., 2005; Pu, 2009; Yu, Ostland, Gong, & Pu, 1999). In LDA, classification equations are formulated based on the pooled within-class covariance matrix of the set of independent variables. An observation is assigned to the class with the highest classification function score (Duda & Hart, 1973). In canonical discriminant analysis one replaces p original variables with up to $g - 1$ derived canonical variates, where g is the number of classes (i.e., 29 tree species; Klecka, 1980). Whereas principal components analysis (PCA) and minimum noise fraction (MNF) summarize the total variability among the set of independent variables, the canonical rotation summarizes the between class variance among g classes. The derived canonical discriminant functions are linear combinations of the original variables where the coefficients maximize the between-group separation. Data reduction with this technique has been successfully applied to remote sensing classification problems including urban tree species discrimination (Alonzo et al., 2013; Pu & Liu, 2011; Zhao & Maclean, 2000). Compared to LDA on p original variables, CDA dramatically improves computational performance and, in the case of limited training data, can avoid the ill-posed problem where the number of variables is greater than the number of observations.

2.5.3. Classification candidate sets

The primary goal of this research was to assess the accuracy with which we could map tree species in a heterogeneous urban forest using fused hyperspectral and lidar data. We attempt to map 29 common species that comprise much of Santa Barbara's canopy area and provide the majority of urban-forest derived ecosystem services. We acknowledge that it is currently impossible to train a classification algorithm on all species present in an urban area. Thus, we trained our CDA classifier to label *all* crowns as one of the 29 common species. At the leaf-type level, the classification was deemed successful when a crown was labeled as a common species with a matching leaf type. For example, if a *Quercus suber* (less common species) was classified as *Quercus agrifolia* (common species) then the leaf-type classification was correct.

In order to separately assess classification accuracy for the 29 common species and the ~70 less common species we subdivided the 2304 total crowns into the four overlapping sets listed below (each corresponding research aim from the Introduction section is also noted):

1) Accuracy for mapping 29 common species (2016 crowns) to the species level (aims #1 & #3)
2) Accuracy for mapping same 29 common species to the leaf-type level (aims #2 & #3)
3) Accuracy for mapping ~70 less common species (288 crowns) to the leaf-type level (aims #2 & #3)
4) Accuracy for mapping ~100 total species (2304 crowns) to the leaf-type level (aims #2 & #3)

2.5.4. Variable combinations

Each candidate set listed in Section 2.5.3 was classified using four different variable subsets. The purpose of adding and holding out variables links with research aim #1: we seek to assess the respective values of hyperspectral data, lidar data, and object-level fusion of both in classification accuracy at the species and leaf-type levels. Prior to classification, for the sake of computational efficiency and methodological consistency, each variable combination was reduced to the maximum number of canonical variates with significant discriminating power ($\alpha = 0.05$). The rotated variable sets used to generate classification equations were thus:

1) All hyperspectral bands (178) and all lidar-based structure variables (28) reduced to 28 canonical variates (hereafter: *CDA-full*).
2) All spectral bands and the subset of 7 lidar variables selected using FFS, reduced to 28 canonical variates (*CDA-7fuse*).

3) All hyperspectral bands (178) reduced to 28 canonical variates (*CDA-spec*).
4) Seven FFS-selected lidar bands reduced to 5 significant canonical variates (*CDA-lid*).

2.5.5. Classification approach

Of the 2304 crowns included in this study, 25 manually delineated crowns from each of the 29 common species, 725 in total, were randomly selected and permanently set aside for model training, leaving 1579 for testing at the leaf-type level and 1291 for testing at the species level. It is necessary to train an object-level classification model using manually delineated crowns in order to assure that the full segment area is composed of one and only one known species (Dalponte et al., 2014). The set of watershed crowns that spatially aligned with the 725 manual crowns was also excluded from the testing to ensure disjoint training and test sets. Ultimately, the 1579 manual crowns and the spatially coincident set of watershed crowns were each classified. The manual crowns were classified in order to evaluate the potential classification errors associated with automatic segmentation (aim #3).

To accommodate the dataset's high within-species structural and spectral variation and so to minimize the impact of outlier crowns on discriminant function generation, the 725 training crowns were subsampled with replacement for each of 50 model runs (mr). That is, for each model run, the discriminant functions were generated using (29 species) × (20 crowns/species) × (an average of 4 spectra per crown) = 2320 fused spectra. Bootstrapping over more model runs (mr = 100) was also investigated but model stability was deemed adequate with mr = 50.

In each model run, discriminant functions were generated based on the current subset of training pixels. This set of 28 ($g - 1$) functions was, in turn, multiplied through the run's training and testing datasets to produce the canonical variates. Pixel level LDA classification was carried out on the test set of canonical variates. Upon completion of each model run, a species label was assigned to each crown based on the pixel majority classification. After completion of all 50 runs, the mode crown-level result was calculated and retained for final map creation and accuracy assessment. Pixel-level classifications were also retained for comparison with results from object-oriented approaches.

The final classifications for the 1579 manual crowns and the spatially coincident watershed segments were mapped in a GIS. A manually delineated ground-reference map with species information for the 29 common species and leaf-type information for the less common species was used for spatial validation. Watershed crown accuracy was assessed only on a canopy-area basis by spatially intersecting the validation map with the classified segments. Percent correctly classified canopy area has been chosen in lieu of the number of correctly classified stems as the primary method for reporting results for two reasons: First, from an urban forest and ecosystem services management perspective it is more important to gather detailed information on species dominant in the local canopy. Second, it is not feasible to conduct stem-count accuracy assessment when the unit of analysis is the potentially-misaligned crown segment. Still, to better understand the utility of lidar for classifying smaller crowns stem count accuracy was assessed for manual crowns.

3. Results

3.1. Crown segmentation accuracy

Assessed against field observations, 83% of the watershed segments contained a single tree stem indicating overall good agreement (Table 3). However, the segmentation accuracy when evaluating only trees from UFORE plots or from Alameda Park decreased to 55%. This is because Alameda Park, in particular, is a highly complex urban forest setting, with significant crown overlap among trees of all sizes and species (Fig. 4). In this type of environment, as evident in Fig. 4, there is clear omission error. This is likely because the window size of the CMM was determined based on a weak relationship between tree height and width. It is particularly noticeable in this figure that the widths of tall but slender palm trees were not modeled well leading to inclusion of neighboring stems in their segments. Still, evaluated against segmentation using the CHM, there was a small overall improvement in segmentation accuracy (1%). The improvement may be more pronounced in densely forested areas but this was not evaluated.

3.2. Forward feature selection of structural variables and spectral bands

Using the cross-validated misclassification rate, 7 variables were selected for classifying manual crowns. The same number was selected for watershed crowns. Six of those variables appear in both selection sets, perhaps indicating that watershed crowns and manual crowns can be classified using the same set of structural metrics (Fig. 5). The only variables differing between the two sets were *h_1* (max crown height) and *h_2* (median height of returns in crown). For simplicity, and given strong intercorrelation, all further analysis was conducted using *h_2* and the six structural variables selected for both manual and watershed crowns. Overall, variables related to tree height and return intensity stand out with respect to their high between-class to within-class variance as quantified by the normalized F-ratio. When taking variable intercorrelation into account, one height metric (*h_2*), one width metric (*w_1*), one height-to-width ratio metric (*hw_rat_2*), two intensity metrics (*int_2* and *int_3*) and two crown porosity metrics (*cp_1* and *cp_3*) were selected in more than 30% of the watershed crown model runs (Fig. 6). That the set of variables selected for each set of objects is nearly identical may highlight the success of segmenting an image largely comprising street trees. It may also indicate that the selected variables are robust to minor aberrations in morphology.

Spectral bands were chosen most consistently from the visible region of the spectrum (VIS, 394–734 nm; Fig. 6). This corresponds with an F-ratio that is relatively high from 400 nm until the red edge at approximately 700 nm. In particular, bands were selected surrounding the green peak between 520 and 590 nm. Selection frequency in that region was driven by discriminatory power and also by relatively low correlation with neighboring bands in the VIS as well as with bands in the shortwave infrared 2 (SWIR2, 2018–2425 nm; Supplementary material S6). The near infrared region (NIR, 744–1313 nm) displayed low F-ratios and yielded one band selected with particular frequency in the liquid water absorption feature centered on 1197 nm. The shortwave infrared 1 region (SWIR1, 1443–1802 nm) and SWIR2 regions yielded high F-ratios but only SWIR1 held bands selected in more than 30% of model runs. The lack of band selection from SWIR2 may be a result of high overall correlation with the VIS (r = 0.84) and the SWIR1 (r = 0.83).

3.3. Classification results

3.3.1. Classification of the 29 common species

The *CDA-7fuse* variable combination yielded the highest overall species-level classification accuracy (83.4% of canopy area, kappa = 82.6) for watershed crowns containing common species (Fig. 7a). Species-level classification accuracy with only hyperspectral data (*CDA-spec*) was 79.2%. Lidar data only (*CDA-lid*) yielded an accuracy of 32.9%. The best fused result using the manual crowns was 85.4%, suggesting minimal impact on classification accuracy by segmentation error (Fig. 8). These object-level results compare favorably to 68%

Table 3
Segmentation accuracy. In bold: 1960 stems were appropriately placed in one watershed crown. Eighty-five segments were without stems.

Stems in segment	0	**1**	2	3	4	5	6	7	8
Segment count	85	**1960**	75	27	10	5	1	1	1

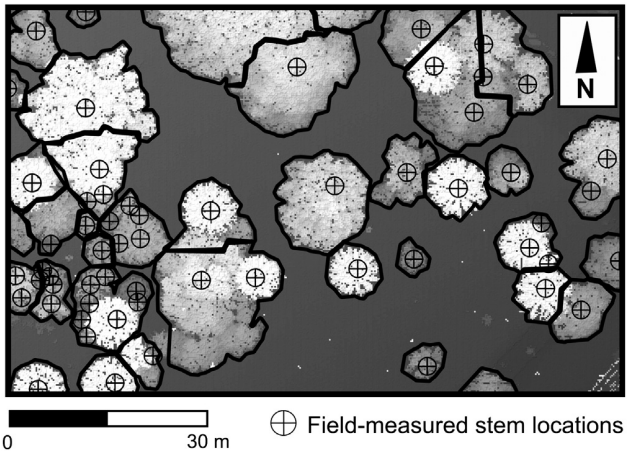

Fig. 4. Subset of Alameda Park lidar canopy height model shaded by height. Watershed segments and field-measured stems. Note the undersegmentation in the densely vegetated southwest corner.

pixel-level accuracy in which a single crown could contain several differently classified pixels. The species map accuracy provided by the best fused model (*CDA-7fuse*) was only 4.2 percentage points (pp) better than the spectral-only model (*CDA-spec*), but there was significant variation when considering the accuracies of individual species (Table 4, Fig. 9; for a larger version of Table 4 with full botanical names see Supplementary material S7).

Large, dense crowned species such as *Ficus microcarpa* (FIMI) were classified well by spectral data alone with an averaged user's and producer's accuracy of 97% (Table 4). Small broadleaf crowns like *Stenocarpus sinuatus* and *Metrosideros excelsa* were poorly classified by spectral data with average accuracies of 24% and 29% respectively. Small crowned species overall were poorly classified by *CDA-spec* and better classified by *CDA-7fuse* (Fig. 9). The classification accuracy of species with the 7 smallest crown sizes increased by an average of 17 pp with incorporation of lidar data. Palm species (ARCU, PHCA, SYRO, WARO) were classified using *CDA-spec* with 43% accuracy and by *CDA-7fuse* to 63%. Conifer species (CUMA, PICA, PIPI2) were classified with 84% accuracy using *CDA-spec* and 85% accuracy with *CDA-7fuse*. The remaining 22 broadleaf species were classified with 73% accuracy with *CDA-spec* and improved to 78% accuracy with *CDA-7fuse*. Several species were classified worse using the *CDA-7fuse* model. Species whose accuracies declined by more than 1 pp included: OLEU, PICA, PHCA, LOCO, SCMO, and STSI.

To further determine the value of adding structural metrics to species classification, we evaluated the success of each variable combination in terms of stem count accuracy. This implies a result that is equally weighted across all species regardless of crown size and could relate to a goal of better understanding the diversity and spatial arrangement of species throughout a city. Stem count accuracy could only be assessed using manual crowns. The stem accuracy with the *CDA-spec* model was 63.0% and increased to a maximum of 71.5% with the *CDA-7fuse* model.

3.3.2. Classification to the leaf-type level

Given the 29 common species, the *CDA-7fuse* model reached 93.5% leaf-type accuracy on watershed crowns and 95.7% accuracy on manual crowns (Fig. 7b). For the same crowns, lidar alone was much more effective at the leaf-type level than at the species level reaching 78.1% accuracy on watershed crowns. Across all (~100) species, *CDA-full* achieved a mapping accuracy of 87.9% to the leaf-type level (Fig. 7c). When mapping just the set of ~70 less common species, the accuracies decreased substantially (Fig. 7d). *CDA-full* mapped watershed segments containing less common species with 59.1% accuracy.

4. Discussion

4.1. Object oriented approach

Within a single tree crown, leaf-level spectral reflectance may vary considerably as a function of biochemistry and water content (Cochrane, 2000; Ustin et al., 2009). In a given AVIRIS pixel there is further within-class spectral variability driven by canopy architecture, exposure of woody biomass, and exposure of underlying substrate (Asner et al., 2008; Clark et al., 2005; Roberts et al., 2004). This variability potentially manifests in a classification result as a single tree crown containing pixels labeled as multiple species. The problem is exacerbated at fine-spatial resolutions since a given pixel's spectral response may deviate significantly from the crown mean spectrum. Our study reaffirms the utility of object-level analysis for relatively fine resolution (3.7 m) hyperspectral imagery. The overall accuracy for mapping the 29 common species using pixels was 68% and increased to 79% using only spectral information but with pixel majority aggregation at the crown-object level. This increase in accuracy at the object level is in line with previous research: van Aardt and Wynne (2007), classifying 3 pine species from AVIRIS imagery, improved their single pixel results by 20 pp (from 65% to 85%) using a 3 × 3 window to compute average spectra prior to classification. Clark et al. (2005) found that, on average, 10% of pixels in each *correctly* labeled crown were misclassified.

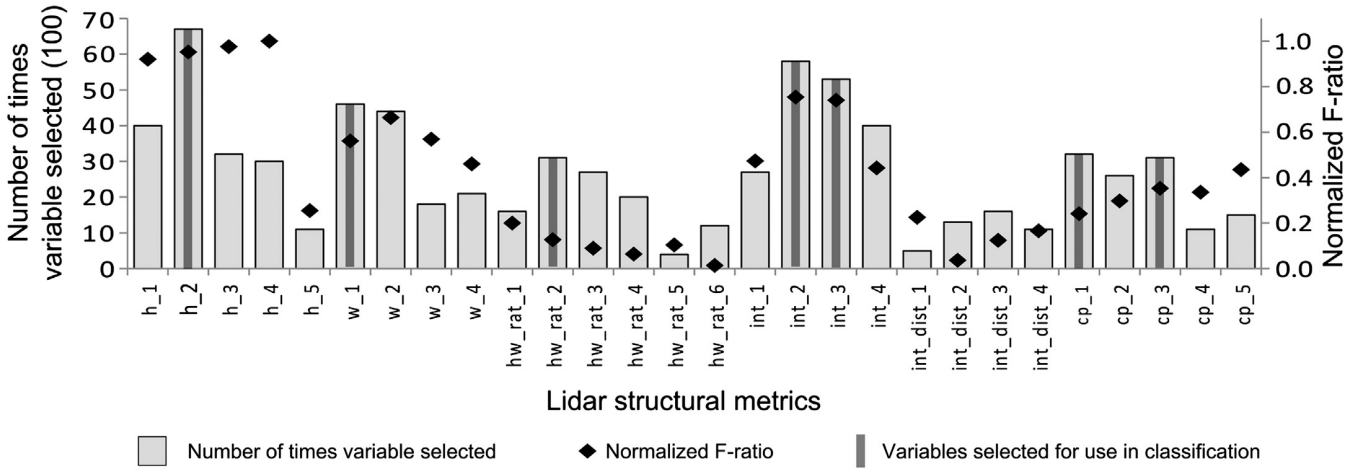

Fig. 5. Column data show the number of times (out of 100 model runs) that each structural variable was selected using forward feature selection (FFS). The black diamonds represent the normalized F-ratio for each variable. The dark gray vertical stripes indicate that a variable was selected for use in classification of watershed crowns.

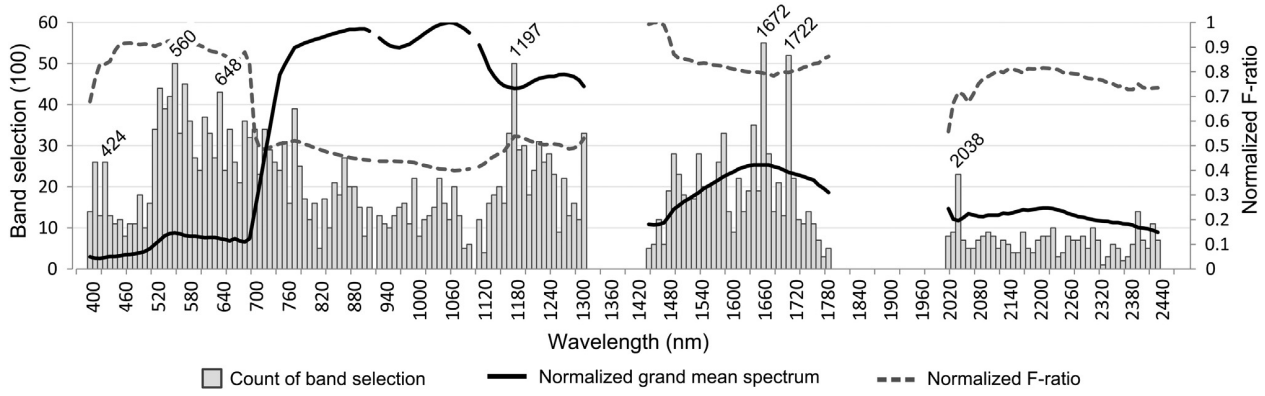

Fig. 6. Column data show the number of times (out of 100 model runs) that each spectral band was selected using forward feature selection (FFS). The black line is the normalized grand mean spectrum for all pixels from common (29) species. The dashed line is the normalized F-ratio for each band.

4.2. Contribution to classification: spectral regions and features

In correspondence with previous research, the hyperspectral imagery in our fusion study was the primary driver of classification accuracy (Fig. 7; Dalponte et al., 2012; Jones et al., 2010; Voss & Sugumaran, 2008). Alonzo et al. (2013) showed that AVIRIS bands spanning the entire solar-reflected region (394 to 2425 nm) are required for accurate classification of urban tree species but that the VIS is particularly important. With 29 urban species, this study reconfirms previous research highlighting the discriminatory power and relatively unique spectral information contributed by green peak bands surrounding 560 nm (Fig. 6; Alonzo et al., 2013; Castro-Esau et al., 2006; Pu, 2009). Bands in the green peak region are commonly related to the expression of xanthophyll cycle pigments (Ustin et al., 2009). Chlorophyll absorption regions near 430 and 642 nm were also repeatedly included. We note a continuation of bands selected in >30% of runs (though a diminution of the F-ratio's value) along the red edge where spectral slope and relative spectral reflectance have been previously employed to discriminate tropical rain forest (Cochrane, 2000) and urban (Pu, 2009; Pu & Landry, 2012) tree species. In contrast to the results of Clark et al. (2005), we find limited discriminatory value in the near infrared (NIR, 744 to 1313 nm) range. It is possible that in their tropical rainforest study area they encountered greater between-class diversity with respect to phenology, LAI, and water status. Our results do correspond to those of Dalponte et al. (2012) who found that the NIR region was poorly suited for discrimination due to very high within-class variance. In our study, the one frequently selected band in the NIR was the prominent liquid water absorption band at 1197 nm. The two most frequently selected bands overall (1672 and 1722 nm) were in the shortwave infrared (SWIR1) region spanning 1443 to 1802 nm. This likely corresponds to species separability driven by variable lignin and cellulose content found in foliar and non-photosynthetic plant matter (Kokaly, Asner, Ollinger, Martin, & Wessman, 2009). The shortwave infrared region (SWIR2) from 2018 to 2425 nm offered little in terms of marginal separability here. A high F-ratio indicates *potential* utility in discrimination but no bands were selected using FFS more than 30% of the time. This may be a product of consistently high sample LAI and leaf water content dampening the viability of lignin-cellulose absorption features (Kokaly et al., 2009). It may also be a product of high correlation among SWIR2, SWIR1, and VIS bands.

4.3. Contribution to classification: structural metrics

The selection of particular structural metrics improved classification accuracy compared to retention of all lidar variables by 2.6 pp, though this difference was not tested for statistical significance (Fig. 7a). Tree height is the single most common lidar variable used in tandem with spectral information as a means to improve classification results (Dalponte et al., 2008; Jones et al., 2010; Koetz, Morsdorf, van der Linder, Curt, & Allgöwer, 2008). This is due in part to its clear utility in facilitating differentiation among spectrally similar tree species but also because it is simple to measure at either the pixel or crown-object scale and perhaps because it is robust to imperfect image segmentation. Our study also found height metrics to be the most important structural variables based on normalized F-ratio (Fig. 5). By the same measure, the second most important variable category

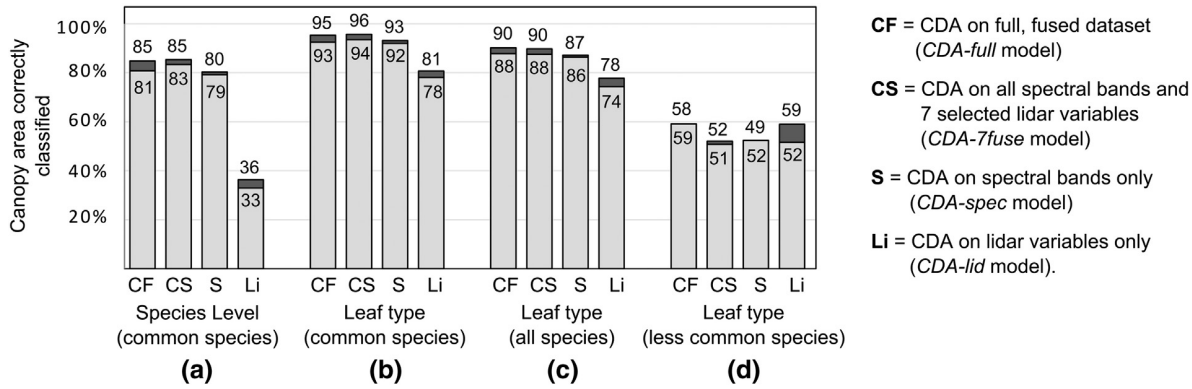

Fig. 7. Canopy area mapping accuracy. Light gray bars show classification accuracy for watershed crowns while darker bars show the improvement when using manual crowns. (a) Species-level accuracy by model for classifying the 29 common species. (b) Leaf-type level accuracy by model for the 29 common species. (c) Leaf-type level accuracy for mapping all (~100) species. (d) Leaf-type level accuracy for mapping the ~70 less common species.

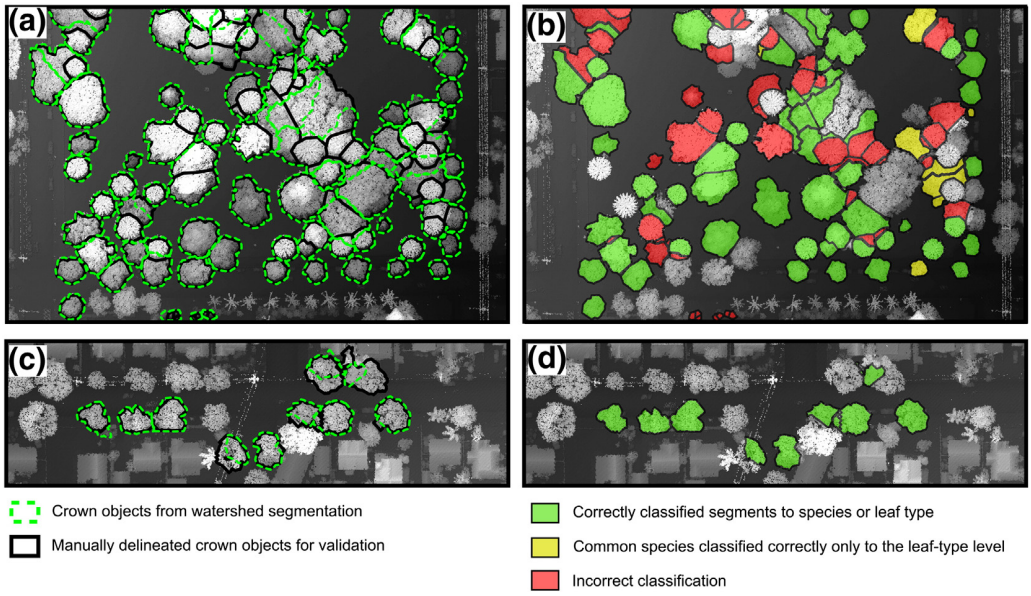

Fig. 8. Subsets of lidar canopy height model showing: (a) Sample of segmentation results in Alameda Park with significant crown overlap. (b) Classification results in Alameda Park. Trees with no color were in the training set and thus not mapped. (c) Sample of street tree segmentation results. (d) Classification of street trees. Trees with no color were either in the training set or not part of the study.

contained return intensity metrics. In particular *int_2* (average intensity below median height of returns in crown) likely describes the arrangement of leaves and branches in a crown's interior while *int_3* (crown surface intensity: 0.25 m spatial resolution) may characterize leaf reflectance values along the crown surface (Kim et al., 2009). A previous study found standard deviation of crown intensity values to be the 2nd most valuable variable (Holmgren & Persson, 2004). They postulated that this metric differentiates densely foliated crowns from those with larger internal gaps. A third grouping of unique variables was those related to crown widths at various heights. Variable *w_1* (crown width at median height of returns in crown) may describe crown morphology in a manner useful for separating upright growth forms from spreading forms. Holmgren & Persson (2004) also found that growth form gave rise to important discriminatory variables. They included *segp*, a summary statistic relating to the shape of a parabola fit to the surface of their study crowns, in their final, successful, classification of two conifer species. Finally, we speculate that *cp_1* (surface heights in 0.25 m grid divided by surface heights in 1 m grid) and *cp_3* (count of returns in 0.5 m vertical slice at 90th percentile height divided by width at that height) are two ways to measure crown porosity.

Table 4
Producer and user accuracies for CDA on the fused dataset compared to CDA on spectral data only. Refer to Fig. 10 for a graphical depiction of the differences in accuracy.

Species	Fused (*CDA-7fuse*)		Spectral only (*CDA-spec*)	
	Prod. (%)	User (%)	Prod. (%)	User (%)
ARCU	65	35	16	34
CICA	84	83	82	74
CUMA	90	91	94	81
EUFI	89	61	58	94
EUGL	93	98	96	91
FIMI	92	100	98	96
GEPA	82	69	39	55
JAMI	95	95	95	93
LIST	87	93	90	77
LOCO	61	75	82	66
MAGR	92	86	89	89
MEEX	42	46	26	32
OLEU	83	94	94	88
PHCA	64	84	72	80
PICA	85	58	84	69
PIPI2	97	89	84	93
PIUN	72	95	91	73
PLRA	83	97	86	86
POGR	92	86	62	82
PYKA	76	58	34	50
QUAG	89	77	80	87
SCMO	32	43	40	41
SCTE	93	94	93	85
STSI	19	18	17	30
SYAU	87	80	87	69
SYRO	36	80	64	17
TISP	99	87	84	88
ULPA	69	84	78	51
WARO	66	76	31	27

It has been shown previously that structural metrics that are ratios of absolute metrics (e.g. *hw_rat_3*: ratio of crown height to width: 90th percentile height) are useful for species discrimination because they are more invariant to life stage and can capture between-species variability in crown morphology (Holmgren & Persson, 2004; Kim et al., 2011). Our urban forest study did not corroborate these findings. The derived structural variables in the set *hw_rat* were purposed to crown form description. However, they offered very limited value to species separability compared to their absolute crown-width analogs. Similarly, the *int_dist* family of variables was created out of the supposed need to normalize for uncalibrated intensity values but also offered minimal discriminatory power. We suggest that ratio metrics were less valuable to this study because the sample set of tree crowns was mostly mature and within-class variance for *absolute* metrics such as heights and widths may have been kept sufficiently low through proactive urban forest management (e.g. pruning, training).

4.4. The impact of segmentation on classification accuracy

The impact of imperfect segmentation on classification accuracy was minimal. The decrease in accuracy of the *CDA-7fuse* classifier when moving from manual crowns to watershed crowns was only 2.0 pp. This is likely the case for several reasons: 1) In this urban study area, the segmentation algorithm successfully isolated 83% of the trees. This is, in part, due to a sample set dominated by street trees, which are easier to delineate than heavily-overlapping private property or park trees. Dalponte et al. (2014) showed a 13 pp reduction in accuracy when

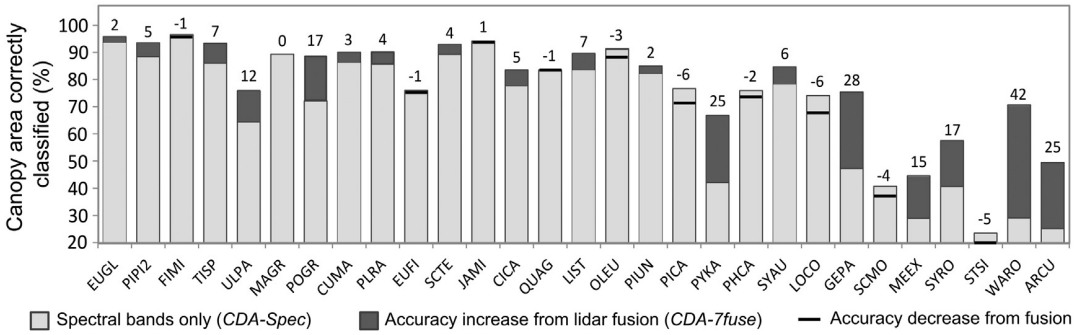

Fig. 9. Classification accuracy by species for spectral bands only (*CDA-spec*) and lidar-hyperspectral fusion (*CDA-7fuse*). Horizontal bars illustrate cases where fusion with lidar reduced accuracy. For species botanical names refer to Table 1. Species are sorted by average crown size with the largest species at left.

classifying three tree species in a more complex boreal forest using automatically-delineated lidar segments compared to manual crowns. 2) The basis on which accuracy was evaluated in this study was canopy *area* (i.e., *not* stem count) correctly classified. In this scenario, large crowns could, for example, be oversegmented yet classified correctly due to the classifier's heavy reliance on pixel-level spectral information. 3) Both the resultant classification map and the initial manual delineation of crowns exist only as 2-dimensional overlays on a gridded CHM. As such, even manual crowns are not perfect representations of 3-D crown morphology and exhibit, in a sense, "segmentation errors" in their own right. Three dimensional segmentation of the lidar point cloud itself, where crown assignment takes place via point clustering at the individual return level, is currently possible (e.g., Ferraz et al., 2012; Reitberger, Schnörr, Krzystek, & Stilla, 2009) and may be useful to implement in future classification projects.

4.5. The utility of lidar data

The overall increase in classification accuracy of 29 common species from the inclusion of lidar structural metrics was 4.2 pp. Previous work in complex forested settings has shown improvements from the addition of lidar to hyperspectral data of 1.1 pp for 23 classes (Dalponte et al., 2008), 1.2 pp for 11 species (Jones et al., 2010), and 6 pp for 6 tree species (Dalponte et al., 2012). There are likely several reasons why the addition of lidar data does not dramatically increase overall accuracy. First and foremost, the structural metrics do not drive species separability as much as spectral bands. In this study, only the height metrics surpassed the VIS spectral bands with respect to their relative F-statistics. Additionally, classification accuracy in this study was assessed in terms of canopy area. Species with large canopies can already be well characterized with only hyperspectral information and an object-oriented approach (e.g. Alonzo et al., 2013). Finally, extraction of accurate structural information is likely most difficult for large crowned species due to frequent intermingling with neighboring crowns, irregular crown shapes, and segmentation error (Chen et al., 2006; Kim et al., 2009). Despite minor increases in *overall* classification accuracy, each of the projects referenced above did demonstrate significant improvements in classification accuracy for certain species.

The value of lidar data is evident for small crowned species (Fig. 9). Of the 8 species whose classification accuracy improved by >10 pp, 6 (ARCU, GEPA, MEEX, PYKA, SYRO, and WARO) were in the bottom half of the sample set in terms of average crown area. The aggregated average crown size for those seven species was 30.4 m^2 compared to an overall average of 78.0 m^2. A particularly notable jump in accuracy (+42 pp) was made when the fused data were used to classify *Washingtonia robusta* (Fig. 10). WARO had the 2nd smallest average crown size and the 2nd highest total tree height. These attributes, on one hand, made WARO difficult to classify using coregistered hyperspectral data both due to its small crown area and because of horizontal crown displacement caused by differing view geometries. On the other hand, these same attributes made WARO structurally unique, and relatively easy to classify upon inclusion of lidar data. This example highlights three key ways in which lidar likely improves classification accuracies. First, with a lidar point density of 22 pulses/m^2 we have the ability to map much smaller discrete objects than with the hyperspectral data alone. Secondly, since the crown objects were generated using the gridded lidar dataset, there is no image registration error. Third, unique crown structural characteristics (e.g., height, crown length, crown shape) are not measureable with optical data alone. With increased availability of fine-spatial resolution hyperspectral data (<1 m) such as AVIRIS Next Generation (Hamlin et al., 2011) or the Carnegie Airborne Observatory (Asner et al., 2007), it will be interesting to see how much classification accuracies can improve even without lidar data.

Some larger crowns were also classified more accurately with *CDA-7fuse* than with spectral data alone. There is evidence that higher crown porosity (possibly relating to lower LAI) may lead to a reduced capacity for accurate classification using spectral data alone. It has been shown that higher LAI strengthens spectral signals in the NIR and portions of the VIS (Asner, 1998). In this study one of the metrics relating to crown porosity was *cp_2*. This metric compares the position of the mean crown height (as a function of tree height and crown base height) to the median height of returns in the crown. Higher numbers suggest a dense upper crown that skews the vertical distribution of lidar returns upwards. Large crowns with the *least* crown porosity by this measure were FIMI and EUGL. FIMI and

Fig. 10. *Washingtonia robusta* (Mexican fan palm).

EUGL were both classified well with spectral data alone (97% and 93% average accuracies respectively) but they were also ranked 3rd and 1st respectively in terms of average crown size. Large and medium crowns with the *highest* porosity were PLRA, PYKA, PICA and ULPA. From the addition of lidar data they gained 4, 25, −6, and 12 pp, respectively. We assume that PICA was ranked highly by this metric more from a combination of upright crown geometry and off-nadir lidar pulses than actual high porosity.

4.6. Classification of less common species

The original choice to map 30 species was made because 80% of Santa Barbara's canopy cover comprises roughly 30 species and there appeared to be diminishing increases in canopy for each additional species added after this point (Supplementary material Figure S1). In Santa Barbara, 23% of the total canopy cover sampled in the UFORE field collection was from two species: the native *Q. agrifolia* (Coast live oak) and the introduced *Syagrus romanzoffiana* (Queen palm). This relationship between species mix and canopy cover may hold in other parts of the country as well. For instance, based on a 2009 UFORE study in Washington, DC (Casey Trees, 2010), roughly the same relationship was established with 25% of canopy composed of two native species: *Fagus grandifolia* (American beech) and *Liriodendron tulipifera* (Tulip tree). In Los Angeles, with a very arid climate and a lack of native canopy dominants, the relationship shifts somewhat but 30 species would still equate to roughly 70% of canopy cover. Given an increase in availability of lidar and hyperspectral datasets, these species–canopy relationships indicate the transferability of the methods established in this paper to conduct similar assessments for the canopy dominants in other, larger cities.

In large cities, with established urban forest management programs, it is feasible to collect training data for and map ~30 species to the species level. However, for those, potentially, hundreds of species with low stem counts representing the remaining 20 or 30% of canopy area, it will be pragmatic to classify only to the leaf-type level. In this study, mapping to the leaf-type level meant modeling the less common species as one of the common species and checking for leaf-type agreement. Over the entire dataset of 2304 crowns (~100 species), leaf-type mapping reached 87.9% accuracy using *CDA-full*. However, when only classifying the ~70 less common species the accuracy declined to 59.1%. We surmise that the low accuracy with which these species were classified is a product of our choice to use a CDA classifier. The classification functions generated were specifically tailored to maximize separability among the input training classes, which did not include the less common species. This leads to a well-tuned classifier for the common species but one that may not be able to capture the variation in the dataset comprising the less common species. Other classification methods may ultimately prove superior for hierarchical classification schemes wherein all trees are classified first to the leaf-type level and then common species are further classified to the species level. For example, Multiple Endmember Spectral Mixture Analysis (MESMA: Roberts et al., 1998) allows for constrained classification based on a target spectrum's similarity to reference spectra such that species not represented in a spectral library would rightly remain unclassified.

5. Conclusions

This research sought to improve species and leaf-type level mapping in the urban forest. We first selected 29 common species that dominate the canopy in Santa Barbara, California and classified them using CDA on combined hyperspectral and high point-density lidar data. We achieved a species-level accuracy among trained species of 83.4%. We mapped the *entire* set of sample crowns, including ~70 less common species, to the leaf-type level with 87.9% accuracy. We believe that this study demonstrates the potential for separating highly overlapping species classes using data fusion at the crown-object level. In an immediate, operational sense, the techniques described in this paper are likely applicable with high accuracy (and perhaps with lower point density lidar data) for discriminating among urban vegetation growth forms (e.g. herbs, shrubs, trees) where simple structural metrics could vastly improve separability when combined with either multi- or hyperspectral data. The data to accomplish this sort of classification are available in many cities today and the results even at this generalized level could inform policy relating to the spatial distribution of urban ecosystem structure and function.

In line with previous research, classification accuracies in this study were bolstered by lidar variables pertaining to tree height, crown morphology, and perhaps the internal arrangement of leaves and branches. In particular, we showed that small crowns and crowns with unique morphological characteristics were more apt to be correctly labeled with the inclusion of structural data. Further, we showed that classification following automated crown segmentation was more accurate than a pixel-level result and the diminution in accuracy introduced from segmentation error was quite small. As many cities have gained access to high-accuracy canopy coverage maps it is a reasonable next step to implement simple crown segmentation algorithms to generate serviceable crown objects for further analysis. Ultimately, the ability to both map dominant canopy species and inventory common but smaller species is important if we're to operationalize remotely sensed urban forest inventory.

Acknowledgments

The authors would like to thank the Naval Postgraduate School for funding this research through grant N00244-11-1-0028, “Quantifying the Structure and Function of an Urban Ecosystem Using Imaging Spectrometry, Thermal Imagery, and Small Footprint LiDAR”. Special thanks also to: Seth Gorelik, Keri Opalk, Alex Sun, Randy Baldwin, and Matt Ritter for their assistance with field data collection; Joe McFadden for supporting field work and helping to refine the manuscript; the City of Santa Barbara for providing ground reference data; Keely Roth and Seth Peterson for help creating and fine-tuning the technical methods; and the four anonymous reviewers for their valuable comments and suggestions.

Appendix A. Supplementary material

Supplementary material for this article can be found online at http://dx.doi.org/10.1016/j.rse.2014.03.018.

References

Alonzo, M., Roth, K., & Roberts, D. (2013). Identifying Santa Barbara's urban tree species from AVIRIS imagery using canonical discriminant analysis. *Remote Sensing Letters, 4*(5), 513–521.

Andersen, H. -E., Reutebuch, S. E., & McGaughey, R. J. (2006). A rigorous assessment of tree height measurements obtained using airborne lidar and conventional field methods. *Canadian Journal of Remote Sensing, 32*(5), 355–366.

Anderson, J., Plourde, L., Martin, M., Braswell, B., Smith, M., Dubayah, R., et al. (2008). Integrating waveform lidar with hyperspectral imagery for inventory of a northern temperate forest. *Remote Sensing of Environment, 112*(4), 1856–1870.

Asner, G. (1998). Biophysical and biochemical sources of variability in canopy reflectance. *Remote Sensing of Environment, 64*(3), 234–253.

Asner, G. P., Knapp, D. E., Kennedy-Bowdoin, T., Jones, M.O., Martin, R. E., Boardman, J., et al. (2007). Carnegie airborne observatory: In-flight fusion of hyperspectral imaging and waveform light detection and ranging for three-dimensional studies of ecosystems. *Journal of Applied Remote Sensing, 1*(1), 1–21.

Asner, G. P., Knapp, D. E., Kennedy-Bowdoin, T., Jones, M.O., Martin, R. E., Boardman, J., et al. (2008). Invasive species detection in Hawaiian rainforests using airborne imaging spectroscopy and LiDAR. *Remote Sensing of Environment, 112*(5), 1942–1955.

Asner, G. P., Mascaro, J., Muller-Landau, H. C., Vieilledent, G., Vaudry, R., Rasamoelina, M., et al. (2011). A universal airborne LiDAR approach for tropical forest carbon mapping. *Oecologia, 168*(4), 1147–1160.

Benz, U. C., Hofmann, P., Willhauck, G., Lingenfelder, I., & Heynen, M. (2004). Multi-resolution, object-oriented fuzzy analysis of remote sensing data for GIS-ready information. *ISPRS Journal of Photogrammetry and Remote Sensing, 58*(3–4), 239–258.

Blaschke, T. (2010). Object based image analysis for remote sensing. *ISPRS Journal of Photogrammetry and Remote Sensing*, *65*(1), 2–16.

Bolund, P., & Hunmammar, S. (1999). Ecosystem services in urban areas. *Ecological Economics*, *29*, 293–301.

Boschetti, M., Boschetti, L., Oliveri, S., Casati, L., & Canova, I. (2007). Tree species mapping with airborne hyperspectral MIVIS data: The Ticino Park study case. *International Journal of Remote Sensing*, *28*, 1251–1261.

Brandtberg, T. (2007). Classifying individual tree species under leaf-off and leaf-on conditions using airborne lidar. *ISPRS Journal of Photogrammetry and Remote Sensing*, *61*(5), 325–340.

Casey Trees (2010). *i-Tree Ecosystem Analysis: Washington, DC.* (URL: http://caseytrees.org/wp-content/uploads/2012/02/report-2010-01-ufore2009.pdf).

Castro-Esau, K., Sanchez-Azofeifa, G., Rivard, B., Wright, S. J., & Quesada, M. (2006). Variability in leaf optical properties of Mesoamerican trees and the potential for species classification. *American Journal of Botany*, *93*(4), 517–530.

Chen, Q., Baldocchi, D., Gong, P., & Kelly, M. (2006). Isolating individual trees in a savanna woodland using small footprint LiDAR data. *Photogrammetric Engineering & Remote Sensing*, *72*(8), 923–932.

Clark, M. L., Roberts, D. A., & Clark, D. B. (2005). Hyperspectral discrimination of tropical rain forest tree species at leaf to crown scales. *Remote Sensing of Environment*, *96*(3–4), 375–398.

Clark, M. L., Roberts, D. A., Ewel, J. J., & Clark, D. B. (2011). Estimation of tropical rain forest aboveground biomass with small-footprint lidar and hyperspectral sensors. *Remote Sensing of Environment*, *115*(11), 2931–2942.

Clarke, L. W., Jenerette, D.G., & Davila, A. (2013). The luxury of vegetation and the legacy of tree biodiversity in Los Angeles, CA. *Landscape and Urban Planning*, *116*, 48–59.

Cochrane, M. (2000). Using vegetation reflectance variability for species level classification of hyperspectral data. *International Journal of Remote Sensing*, *21*(10), 2075–2087.

Dalponte, M., Bruzzone, L., & Gianelle, D. (2008). Fusion of hyperspectral and LIDAR remote sensing data for classification of complex forest areas. *IEEE Transactions on Geoscience and Remote Sensing*, *46*(5), 1416–1427.

Dalponte, M., Bruzzone, L., & Gianelle, D. (2012). Tree species classification in the Southern Alps based on the fusion of very high geometrical resolution multispectral/hyperspectral images and LiDAR data. *Remote Sensing of Environment*, *123*, 258–270.

Dalponte, M., Ørka, H. O., Ene, L. T., Gobakken, T., & Næsset, E. (2014). Tree crown delineation and tree species classification in boreal forests using hyperspectral and ALS data. *Remote Sensing of Environment*, *140*, 306–317.

Dennison, P. E., & Roberts, D. A. (2003). The effects of vegetation phenology on endmember selection and species mapping in southern California chaparral. *Remote Sensing of Environment*, *87*(2), 295–309.

Digabel, H., & Lantuéjoul, C. (1978). Iterative algorithms. *Proc. 2nd European Symp. Quantitative analysis of microstructures in material science. Biology and Medicine*, *Vol. 19, No. 7.* (pp. 8). Stuttgart, West Germany: Riederer Verlag.

Duda, R. O., & Hart, P. E. (1973). *Pattern classification and scene analysis.* New York: John Wiley and Sons, Inc.

Edson, C., & Wing, M. G. (2011). Airborne light detection and ranging (LiDAR) for individual tree stem location, height, and biomass measurements. *Remote Sensing*, *3*(12), 2494–2528.

Escobedo, F. J., & Nowak, D. J. (2009). Spatial heterogeneity and air pollution removal by an urban forest. *Landscape and Urban Planning*, *90*(3–4), 102–110.

Ferraz, A., Bretar, F., Jacquemoud, S., Gonçalves, G., Pereira, L., Tomé, M., et al. (2012). 3-D mapping of a multi-layered Mediterranean forest using ALS data. *Remote Sensing of Environment*, *121*, 210–223.

Franke, J., Roberts, D. A., Halligan, K., & Menz, G. (2009). Hierarchical multiple endmember spectral mixture analysis (MESMA) of hyperspectral imagery for urban environments. *Remote Sensing of Environment*, *113*(8), 1712–1723.

Green, R., Eastwood, M., Sarture, C., Chrien, T., Aronsson, M., Chippendale, B., et al. (1998). Imaging spectroscopy and the airborne visible/infrared imaging spectrometer (AVIRIS). *Remote Sensing of Environment*, *65*(3), 227–248.

Hamlin, L., Green, R. O., Mouroulis, P., Eastwood, M., Wilson, D., Dudik, M., et al. (2011). Imaging spectrometer science measurements for terrestrial ecology: AVIRIS and new developments. *Aerospace Conference, 2011 IEEE.*

Heinzel, J., & Koch, B. (2011). Exploring full-waveform LiDAR parameters for tree species classification. *International Journal of Applied Earth Observation and Geoinformation*, *13*(1), 152–160.

Hoffbeck, J., & Landgrebe, D. (1996). Classification of remote sensing images having high spectral resolution. *Remote Sensing of Environment*, *57*, 119–126.

Holmgren, J., & Persson, Å. (2004). Identifying species of individual trees using airborne laser scanner. *Remote Sensing of Environment*, *90*(4), 415–423.

Holmgren, J., Persson, Å., & Söderman, U. (2008). Species identification of individual trees by combining high resolution LiDAR data with multi-spectral images. *International Journal of Remote Sensing*, *29*(5), 1537–1552.

Jones, T. G., Coops, N. C., & Sharma, T. (2010). Assessing the utility of airborne hyperspectral and LiDAR data for species distribution mapping in the coastal Pacific Northwest, Canada. *Remote Sensing of Environment*, *114*(12), 2841–2852.

Kim, S., Hinckley, T., & Briggs, D. (2011). Classifying individual tree genera using stepwise cluster analysis based on height and intensity metrics derived from airborne laser scanner data. *Remote Sensing of Environment*, *115*(12), 3329–3342.

Kim, S., Mcgaughey, R. J., Andersen, H., & Schreuder, G. (2009). Tree species differentiation using intensity data derived from leaf-on and leaf-off airborne laser scanner data. *Remote Sensing of Environment*, *113*(8), 1575–1586.

Klecka, W. (1980). *Discriminant analysis.* Beverly Hills: Sage Publications.

Koetz, B., Morsdorf, F., van der Linder, S., Curt, T., & Allgöwer, B. (2008). Multi-source land cover classification for forest fire management based on imaging spectrometry and LiDAR data. *Forest Ecology and Management*, *256*, 263–271.

Kokaly, R. F., Asner, G. P., Ollinger, S. V., Martin, M. E., & Wessman, C. A. (2009). Characterizing canopy biochemistry from imaging spectroscopy and its application to ecosystem studies. *Remote Sensing of Environment*, *113*, S68–S91.

Latifi, H., Fassnacht, F., & Koch, B. (2012). Forest structure modeling with combined airborne hyperspectral and LiDAR data. *Remote Sensing of Environment*, *121*, 10–25.

Lee, J. H., & Bang, K. W. (2000). Characterization of urban stormwater runoff. *Water Research*, *34*(6), 1773–1780.

Lim, K., Treitz, P., Wulder, M., St-Onge, B., & Flood, M. (2003). LiDAR remote sensing of forest structure. *Progress in Physical Geography*, *27*(1), 88–106.

Liu, L., Pang, Y., Fan, W., Li, Z., & Li, M. (2011). Fusion of airborne hyperspectral and LiDAR data for tree species classification in the temperate forest of northeast China. *Geoinformatics, 2011 19th International Conference on Geoinformatics*, 1–5.

Lucas, R. M., Lee, A.C., & Bunting, P. J. (2008). Retrieving forest biomass through integration of CASI and LiDAR data. *International Journal of Remote Sensing*, *29*(5), 1553–1577.

Lyytimäki, J., Petersen, L. K., Normander, B., & Bezák, P. (2008). Nature as a nuisance? Ecosystem services and disservices to urban lifestyle. *Environmental Sciences*, *5*(3), 161–172.

MacFaden, S. W., O'Neil-Dunne, J. P., Royar, A.R., Lu, J. W., & Rundle, A. G. (2012). High-resolution tree canopy mapping for New York City using LIDAR and object-based image analysis. *Journal of Applied Remote Sensing*, *6*(1).

Manning, W. J. (2008). Plants in urban ecosystems: Essential role of urban forests in urban metabolism and succession toward sustainability. *The International Journal of Sustainable Development and World Ecology*, *15*(4), 362–370.

Martin, M. E., Newman, S. D., Aber, J.D., & Congalton, R. G. (1998). Determining forest species composition using high spectral resolution remote sensing data. *Remote Sensing of Environment*, *65*, 249–254.

Mascaro, J., Detto, M., Asner, G. P., & Muller-Landau, H. C. (2011). Evaluating uncertainty in mapping forest carbon with airborne LiDAR. *Remote Sensing of Environment*, *115*(12), 3770–3774.

McCarthy, H. R., & Pataki, D. E. (2010). Drivers of variability in water use of native and non-native urban trees in the greater Los Angeles area. *Urban Ecosystems*, *13*(4), 393–414.

McGee, J. A., Day, S. D., Wynne, R. H., & White, M. B. (2012). Using geospatial tools to assess the urban tree canopy: Decision support for local governments. *Journal of Forestry*, *110*(5), 275–286.

McPherson, E. G., Simpson, J. R., Xiao, Q., & Wu, C. (2011). Million trees Los Angeles canopy cover and benefit assessment. *Landscape and Urban Planning*, *99*(1), 40–50.

Morsdorf, F., Kotz, B., Meier, E., Itten, K., & Allgower, B. (2006). Estimation of LAI and fractional cover from small footprint airborne laser scanning data based on gap fraction. *Remote Sensing of Environment*, *104*(1), 50–61.

Myint, S. W., Brazel, A., Okin, G., & Buyantuyev, A. (2010). Combined effects of impervious surface and vegetation cover on air temperature variations in a rapidly expanding desert city. *GIScience & Remote Sensing*, *47*(3), 301–320.

Myint, S. W., Gober, P., Brazel, A., Grossman-Clarke, S., & Weng, Q. (2011). Per-pixel vs. object-based classification of urban land cover extraction using high spatial resolution imagery. *Remote Sensing of Environment*, *115*(5), 1145–1161.

Næsset, E., & Gobakken, T. (2008). Estimation of above- and below-ground biomass across regions of the boreal forest zone using airborne laser. *Remote Sensing of Environment*, *112*(6), 3079–3090.

Nowak, D., Crane, D., Stevens, J., Hoehn, R., Walton, J., & Bond, J. (2008). A ground-based method of assessing urban forest structure and ecosystem services. *Arboriculture & Urban Forestry*, *34*(6), 347–358.

Ørka, H. O., Gobakken, T., Næsset, E., Ene, L., & Lien, V. (2012). Simultaneously acquired airborne laser scanning and multispectral imagery for individual tree species identification. *Canadian Journal of Remote Sensing*, *38*(02), 125–138.

Ørka, H. O., Næsset, E., & Bollandsås, O. M. (2009). Classifying species of individual trees by intensity and structure features derived from airborne laser scanner data. *Remote Sensing of Environment*, *113*(6), 1163–1174.

Pohl, C., & Van Genderen, J. (1998). Review article Multisensor image fusion in remote sensing: concepts, methods and applications. *International Journal of Remote Sensing*, *19*(5), 37–41.

Popescu, S., Wynne, R., & Nelson, R. (2003). Measuring individual tree crown diameter with lidar and assessing its influence on estimating forest volume and biomass. *Canadian Journal of Remote Sensing*, *29*(5), 564–577.

Pu, R. (2009). Broadleaf species recognition with in situ hyperspectral data. *International Journal of Remote Sensing*, *30*(11), 2759–2779.

Pu, R., & Landry, S. (2012). A comparative analysis of high spatial resolution IKONOS and WorldView-2 imagery for mapping urban tree species. *Remote Sensing of Environment*, *124*, 516–533.

Pu, R., & Liu, D. (2011). Segmented canonical discriminant analysis of in situ hyperspectral data for identifying 13 urban tree species. *International Journal of Remote Sensing*, *32*(8), 2207–2226.

Reitberger, J., Schnörr, C., Krzystek, P., & Stilla, U. (2009). 3D segmentation of single trees exploiting full waveform LIDAR data. *ISPRS Journal of Photogrammetry and Remote Sensing*, *64*(6), 561–574.

Richter, R., & Schlaepfer, D. (2002). Geo-atmospheric processing of airborne imaging spectrometry data. Part 2: Atmospheric/topographic correction. *International Journal of Remote Sensing*, *23*, 37–41.

Roberts, D. A., Gardner, M., Church, R., Ustin, S., Scheer, G., & Green, R. O. (1998). Mapping chaparral in the Santa Monica Mountains using multiple endmember spectral mixture models. *Remote Sensing of Environment*, *65*(3), 267–279.

Roberts, D. A., Ustin, S. L., Ogunjemiyo, S., Greenberg, J., Dobrowski, S. Z., Chen, J., et al. (2004). Spectral and structural measures of northwest forest vegetation at leaf to landscape scales. *Ecosystems*, *7*(5), 545–562.

Rouse, J. W., Haas, R. S., Schell, J. A., & Deering, D. W. (1973). Monitoring vegetation systems in the Great Plains with ERTS. *Proceedings, 3rd ERTS symposium, 1*. (pp. 48–62).
Schneider, A., Friedl, M. A., & Potere, D. (2010). Mapping global urban areas using MODIS 500-m data: New methods and datasets based on "urban ecoregions". *Remote Sensing of Environment, 114*(8), 1733–1746.
Shrestha, R., & Wynne, R. H. (2012). Estimating biophysical parameters of individual trees in an urban environment using small footprint discrete-return imaging lidar. *Remote Sensing, 4*(12), 484–508.
Simpson, J. (2002). Improved estimates of tree-shade effects on residential energy use. *Energy and Buildings, 34*(10), 1067–1076.
Solberg, S., Brunner, A., Hanssen, K. H., Lange, H., Næsset, E., Rautiainen, M., et al. (2009). Mapping LAI in a Norway spruce forest using airborne laser scanning. *Remote Sensing of Environment, 113*(11), 2317–2327.
Swatantran, A., Dubayah, R., Roberts, D., Hofton, M., & Blair, J. B. (2011). Mapping biomass and stress in the Sierra Nevada using lidar and hyperspectral data fusion. *Remote Sensing of Environment, 115*(11), 2917–2930.
Tang, H., Dubayah, R., Swatantran, A., Hofton, M., Sheldon, S., Clark, D. B., et al. (2012). Retrieval of vertical LAI profiles over tropical rain forests using waveform lidar at La Selva, Costa Rica. *Remote Sensing of Environment, 124*, 242–250.
UN-Habitat (2011). *Cities and climate change: Global report on human settlements*. United Nations Human Settlements Programme.
Urban, J. (1992). Bringing order to the technical dysfunction within the urban forest. *Journal of Arboriculture, 18*(2), 85–90.
Ustin, S. L., Gitelson, A., Jacquemoud, S., Schaepman, M., Asner, G. P., Gamon, J., et al. (2009). Retrieval of foliar information about plant pigment systems from high resolution spectroscopy. *Remote Sensing of Environment, 113*, S57–S67.
van Aardt, J., & Wynne, R. H. (2007). Examining pine spectral separability using hyperspectral data from an airborne sensor: An extension of field-based results. *International Journal of Remote Sensing, 28*(1).
Vaughn, N. R., Moskal, L. M., & Turnblom, E. C. (2012). Tree species detection accuracies using discrete point lidar and airborne waveform lidar. *Remote Sensing, 4*(2), 377–403.
Voogt, J. A. (2002). Urban heat island. In I. Douglas (Ed.), *Causes and consequences of global environmental change, Vol. 3*. (pp. 660–666). Chichester: John Wiley & Sons, Ltd.
Voss, M., & Sugumaran, R. (2008). The seasonal effect on tree species classification in an urban environment using hyperspectral data, LiDAR, and an object-oriented approach. *Sensors, 8*(5), 3020–3036.
Welch, R. (1982). Spatial resolution requirements for urban studies. *International Journal of Remote Sensing, 3*(2), 139–146.
Xiao, Q., Ustin, S. L., & McPherson, E. G. (2004). Using AVIRIS data and multiple-masking techniques to map urban forest tree species. *International Journal of Remote Sensing, 25*(24), 5637–5654.
Yang, C., Everitt, J. H., Fletcher, R. S., Jensen, R. R., & Mausel, P. W. (2009). Evaluating AISA + hyperspectral imagery for mapping black mangrove along the South Texas Gulf Coast. *Photogrammetric Engineering & Remote Sensing, 75*(4), 425–435.
Yao, W., Krzystek, P., & Heurich, M. (2012). Tree species classification and estimation of stem volume and DBH based on single tree extraction by exploiting airborne full-waveform LiDAR data. *Remote Sensing of Environment, 123*, 368–380.
Youngentob, K. N., Roberts, D. A., Held, A. A., Dennison, P. E., Jia, X., & Lindenmayer, D. B. (2011). Mapping two Eucalyptus subgenera using multiple endmember spectral mixture analysis and continuum-removed imaging spectrometry data. *Remote Sensing of Environment, 115*(5), 1115–1128.
Yu, B., Ostland, M., Gong, P., & Pu, R. (1999). Penalized discriminant analysis of in situ hyperspectral data for conifer species recognition. *IEEE Transactions on Geoscience and Remote Sensing, 37*(5), 2569–2577.
Zhang, C., & Qiu, F. (2012). Mapping individual tree species in an urban forest using airborne lidar data and hyperspectral imagery. *Photogrammetric Engineering & Remote Sensing, 78*(10), 1079–1087.
Zhao, G., & Maclean, A. (2000). A comparison of canonical discriminant analysis and principal component analysis for spectral transformation. *Photogrammetric Engineering & Remote Sensing, 66*(7), 841–847.
Zhao, K., & Popescu, S. (2009). Lidar-based mapping of leaf area index and its use for validating GLOBCARBON satellite LAI product in a temperate forest of the southern USA. *Remote Sensing of Environment, 113*(8), 1628–1645.